Nanoscale imaging of surface acoustic waves by scanning tunneling microscopy

R. Koch[a] and Jianshu Yang[b]
Paul-Drude-Institut für Festkörperelektronik, Hausvogteiplatz 5-7, D-10117 Berlin, Germany

(Received 16 November 2004; accepted 14 March 2005; published online 9 May 2005)

The scanning tunneling microscope (STM) has proven to be a powerful technique for probing surface acoustic waves (SAWs) with high spatial resolution. Here we use our ultrahigh-vacuum SAW-STM to investigate a Rayleigh wave excited in $LiNbO_3$ with emphasis laid on the SAW-induced signals at steps that are only a few atomic layers high. Our study reveals that on the length scale of a few nanometer the description of the amplitude and phase contrast by a plain geometrical model fails and a variety of other mechanisms decisively affect the SAW-induced signal. At steps the lateral surface movement due to the SAW may play an important role. For larger step inclination angles also the shape of the STM tip as well as tip-surface interactions become relevant, which may even drive a SAW-induced movement of the tip apex. © *2005 American Institute of Physics*. [DOI: 10.1063/1.1903102]

I. INTRODUCTION

Surface acoustic waves (SAWs) are a standard probe in materials science[1] because the dynamics of the surface motion contains important information on surface and subsurface elastic properties and material structure. Commonly, the elastic constants of bulk crystals and thin films are determined by optical methods, which measure the propagation time of the SAW over a distance of many wavelengths, thus yielding the phase velocity averaged over the propagation path.[2] The spatial resolution of optical detection techniques is limited by the laser beam size. Employing lock-in and mixing techniques, Chilla *et al.*[3] demonstrated that scanning probe techniques—despite their large response times—are sensitive to high-frequency (HF) SAW fields ($\sim$10 MHz $\rightarrow \sim$GHz) as well. In the last years the unique spatial resolution of the scanning tunneling microscope[4–6] (STM) and the atomic force microscope[7–9] (AFM) was frequently utilized to investigate the amplitude and phase of SAWs locally on a nanometer length scale.

Recently we have shown that amplitude and phase images obtained with an UHV SAW-STM on highly corrugated surfaces can be described quantitatively by the geometrical model of Chilla *et al.*[3,10] (see Sec. IV A). From the comparison of experimental and simulated amplitude and phase images even the eccentricity of the oscillation ellipse of the SAW-induced surface movement can be determined from surface areas as small as 3×3 nm^2.[5] Furthermore, we found evidence that also the mixing signal measured at nanoscale features such as step edges contains information on the eccentricity.[6] Since the eccentricity is directly related to the elastic constants, these results indeed are very promising as the local elastic properties at grain boundaries, dislocations, and other crystal defects eventually come within reach.

Here we report on a detailed analysis of the SAW-STM experiments focusing on the imaging at steps that are only a few atomic layers high. Our study corroborates that the plain geometrical model fails, when the feature size reaches the length scale of a few nanometer, and several other mechanisms affecting the detected SAW signal have to be considered as well. At steps, the lateral component of the surface movement becomes more important. Furthermore, it turns out that particularly at steps with heights larger than the average tunneling distance and large inclination angles the shape of the STM tip as well as tip-surface interactions become relevant, which may even drive a SAW-induced movement of the tip apex.

II. EXPERIMENT

The experiments presented here were performed in an UHV system consisting of separate chambers for sample preparation and SAW-STM investigation (base pressure $\leqslant 2\times10^{-10}$). The UHV SAW-STM (see Ref. 11) is based on a commercial Omicron STM-1 and has been modified by adding an UHV-compatible high-frequency wiring system for SAW excitation and signal detection up to 1 GHz. The substrate is a piezoelectric single-crystal, *Y*-cut $LiNbO_3$, which carries a lithographically fabricated five-finger floating-electrode unidirectional transducer (700×500 μm^2) for exciting a Rayleigh wave with a resonance frequency of 246 MHz. The substrate is mounted onto a sample holder which allows for versatile sample transfer into and within the UHV system. A 100-nm-thick conducting gold film, which serves as the conducting layer for the SAW-STM experiment, was deposited *in situ* at a temperature of 400 °C and a deposition rate of 0.1 nm/s.

The experimental setup of a SAW-STM is schematically illustrated in Fig. 1. The STM tip is positioned above the conducting film on the piezoelectric sample, which is located in the propagation region of the SAW excited by the interdigital transducer (IDT) on the left. The SAW-induced surface oscillations at the frequency ω_{SAW} give rise to a HF contribution in the tunneling current between the tip and con-

[a]Electronic mail: koch@pdi-berlin.de
[b]Present address: Institute of Materials Research and Engineering, 3 Research Link Singapore 117602.

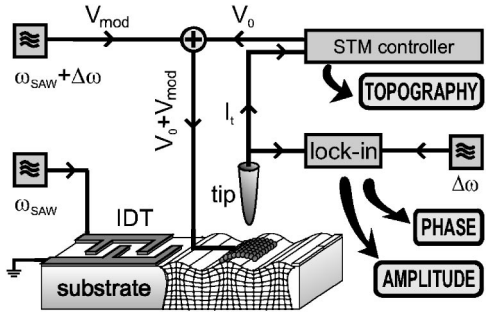

FIG. 1. Experimental setup of the SAW-STM for the measurement of SAW motion. The SAW-induced tunneling current modulation at the frequency ω_{SAW} is mixed with the modulation of the tunneling voltage ($\omega_{SAW}+\Delta\omega$) at the nonlinear current/distance characteristics of the tunneling gap. A lock-in amplifier extracts amplitude and phase of the resulting difference frequency signal ($\Delta\omega$), which both are recorded in addition to the topography and reflect amplitude and phase of the SAW.

ducting layer. The HF component is mixed at the nonlinear current distance characteristics of the tunneling gap with a HF voltage V_{mod} of frequency $\omega_{SAW}+\Delta\omega$, which is added to the common dc tunneling voltage V_0. The difference frequency $\Delta\omega$ is chosen to be in the kilohertz range (40–100 kHz) in order to easily analyze the mixing signal by conventional STM electronics and lock-in technique. It has the same phase and an amplitude proportional to that of the SAW. In our experiments the mixing signal is recorded simultaneously with topography.

III. SAW-STM AT STEPS

A Rayleigh wave on *Y*-cut $LiNbO_3$ was investigated by SAW-STM. Figure 2(a), left is a topographical STM image of the 100-nm-thick Au film showing atomically flat (111) terraces; the data of the right image are differentiated. The steps terminating the terraces denoted by M_i in Fig. 2(a) exhibit heights of 0.5–1.5 nm and ascend from bottom left to top right. Step S_1 vertically crossing the large terrace in the center of Fig. 2(a) and step S_2 are of single height ($\sim$0.2 nm). Note that S_1 exhibits angles of 60° and 120° with respect to the other steps.

The amplitude and phase of the tunneling signal at the difference frequency between the SAW-induced surface oscillation and high-frequency bias voltage are extracted simultaneously from the tunneling current while scanning the topography. Corresponding gray scale images are displayed in Figs. 2(b) and 2(c). Obviously the signals of amplitude and phase are convoluted with topographical information; therefore, the overall morphology displayed in Fig. 2(a) can be easily recognized too. Note that the structural features are even more pronounced in amplitude and phase images, comparable with the differentiated topography in Fig. 2(a), right. On the terraces both amplitude and phase are uniform, and significant changes are observed at the steps (brighter contrast corresponds to larger amplitude and phase signals). The amplitude signal at multisteps is increased by 60%–80% compared to the flat terrace, the phase by 90°–100°. Amplitude and phase measured at different multisteps depend only slightly on the step height varying only by about 5°. On the other hand, the phase difference between monosteps S_i and

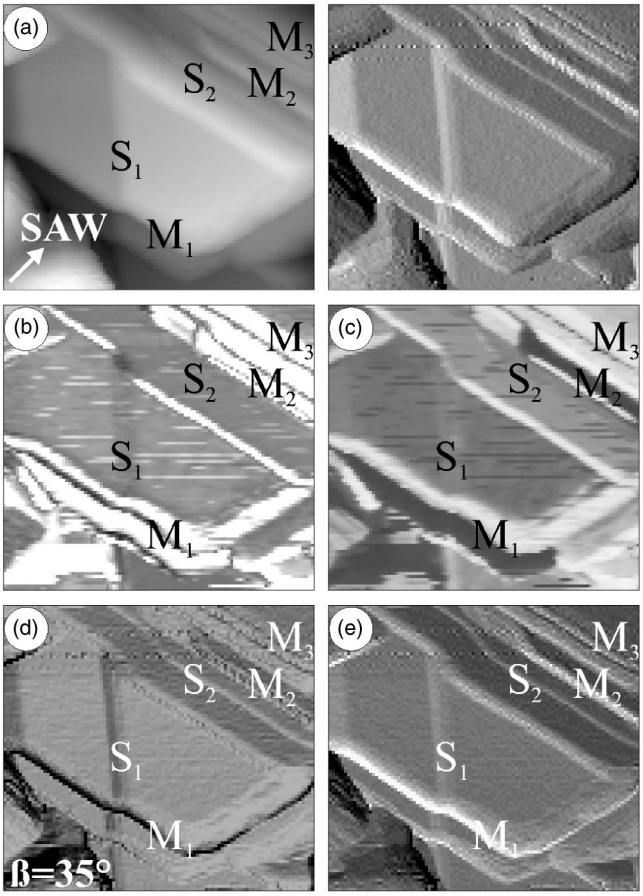

FIG. 2. (a) 40×40 nm^2 topview (left) and differentiated topview image (right) of a 100-nm-thick Au film on *Y*-cut $LiNbO_3$ as well as (b) amplitude and (c) phase image of a Rayleigh wave, all recorded simultaneously with the SAW-STM; single and multiple steps are marked by S_i and M_i, respectively. (d) and (e) are simulated amplitude and phase images calculated with an eccentricity of $\beta=35°$ for the oscillation ellipse, which is the theoretical value for the Rayleigh wave in this system.

the terrace is considerably smaller (only 9°) and the amplitude is even smaller at the step. It is also notable that the step width is generally wider in amplitude and phase images than in topography.

IV. ANALYSIS

A. Geometric model described in Refs. 3 and 10

As found previously in SAW-STM experiments of corrugated surfaces the geometrical projection of the oscillation ellipse is monitored by the STM tip,[3,10] since the electrons tunnel mainly along the shortest line between the tip apex and sample surface. Amplitude A and phase φ of the mixing signal therefore depend on both the local inclination of the surface with respect to the propagation direction of the SAW, and the eccentricity of the oscillation ellipse $\beta=\arctan(u_1/u_3)$; u_1 and u_3 are the longitudinal and transverse displacement amplitudes, respectively, with $u_0=\sqrt{u_1^2+u_3^2}$. Introducing spherical coordinates with respective polar and azimuthal angles Θ and Φ one obtains (see Ref. 10)

$$A \propto u_0\sqrt{\sin^2\beta\cos^2\Phi\sin^2\Theta+\cos^2\beta\cos^2\Theta}, \qquad (1)$$

$$\varphi = \arctan(\tan\beta \cos\Phi \tan\Theta). \quad (2)$$

Whereas on top of a flat horizontal terrace ($\Theta = 0°$) only the normal component ($u_3 = u_0 \cos\beta$) of the oscillation trajectory is measured, the in-plane component ($u_1 = u_0 \sin\beta$) is contributing, in addition, at inclined facets. Note that the time between setting an x/y position and readout of the z value and the SAW signals was 0.03 s. The lock-in amplifier therefore averages over about 7×10^6 oscillation cycles and the amplitude and phase images are uniform within terraces. Due to the small length scale of typical STM images compared with the SAW wavelength (≈ 15 μm) the relative phase shift induced by the linear SAW phase delay with increasing distance from the IDT is about 1° for the entire image of Fig. 2(a).

Using Eqs. (1) and (2), we simulated amplitude and phase images for different eccentricity values β by taking the STM topography of Fig. 2(a) as an input parameter (for details see Refs. 3 and 5). Best agreement with experiment is achieved for $\beta = 30° \mp 40°$ [e.g., Figs. 2(d) and 2(e)], i.e., for eccentricity values comparable to that of the Rayleigh wave ($\beta_{\text{Rayleigh}} = 35.1°$). As expected, also the simulated amplitude and phase images include the main structural features of the topography. In accordance with the experiment [Fig. 2(b) and 2(c)], the contrast in both the amplitude and phase is uniform within the terraces and enhanced at the edges of the multisteps; the amplitude at the single step S_i, on the other hand, is slightly reduced and the phase slightly enhanced.

However, although the simulated amplitude and phase images qualitatively reproduce the main structural features of the topography, there are significant deviations when quantitatively analyzing the results. In particular, the enhanced amplitude signal observed experimentally at the steps is not consistent with the simulations. Figure 3 displays the relative amplitude A/A_h of different facets, A_h being the amplitude on a horizontal plane, as well as the respective phase variation calculated for our Rayleigh wave. The orientation of the facet planes is described by the polar angle Θ of the surface normal as well as by the azimuth Φ measured from the propagation direction of the SAW (along x axis). According to the geometric model the amplitude of an inclined surface is always smaller than that of a horizontal plane ($\Theta = 0$). Azimuthal rotation leads to a further decrease of A. According to the simulations also the phase is shifted, the more the larger tilt against the horizontal plane. However, the experimental phase shift at the steps is considerably higher than the calculated one, e.g., 90°–100° at the multisteps compared with a calculated value of 42°, or 9° at the single step S_1 which compares with 4.5° in the simulation.

B. Nanoscale feature size

In a recent study[6] we found that the geometrical model proposed by Chilla *et al.*[3,10] is no longer applicable, when the features of interest become comparable in size with the area from which the majority of the tunneling current is collected. In that case also the lateral movement of the nanoscale object contributes significantly to the the tunneling current. In order to get a quantitative estimate of the resulting mixing signal, we consider the tunneling at a straight step which separates two otherwise extended flat terraces. The step of height h runs perpendicular to the SAW propagation direction (cf. Fig. 4). The entire surface, including the step, oscillates with the frequency ω of the SAW, with each point following a trajectory defined by the longitudinal (u_1) and vertical (u_3)

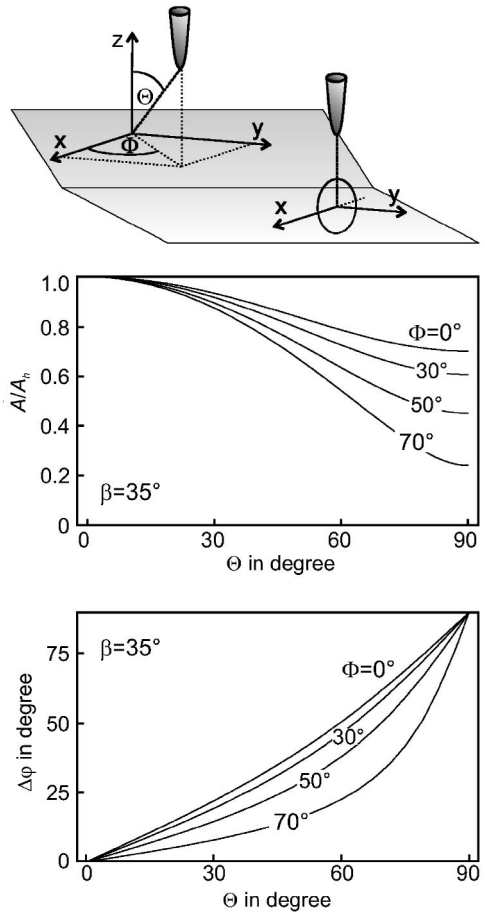

FIG. 3. Relative amplitude A/A_h and phase-shift $\Delta\varphi$ as a function of the inclination angle Θ for different azimuthal tilts Φ calculated by Eqs. (1) and (2), respectively; polar and azimuthal angles Θ and Φ are illustrated in the sketch; A and A_h are the amplitude of the mixing signal at the horizontal and inclined plane, respectively.

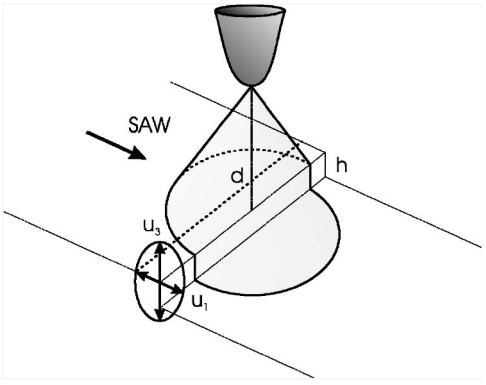

FIG. 4. Schematic illustration of the tunneling current arising at an an oscillating step while being scanned by the STM tip at a distance d: The step of height h separates two extended flat terraces and runs perpendicular to the propagation direction of the SAW. The entire surface, including the step, oscillates with the frequency ω of the SAW, with each point following a trajectory defined by the longitudinal (u_1) and vertical (u_3) SAW amplitudes.

SAW amplitudes. When the STM tip is scanning on the terrace, far away from the step, the tunneling current is modulated only by the vertical oscillation component (i.e., $\propto u_3 \cos \omega t$); the longitudinal movement of the surface leaves the overall tunneling area unchanged and therefore does not lead to a change in the tunneling current. When the tip scans the step edge, most of the tunneling current arises from the upper terrace due to the exponential distance dependence. For instance, at monosteps of Au(111) with a height of 0.236 nm, the current from the upper terrace is more than ten times larger than that of the lower terrace. Due to the SAW-induced lateral movement of the step edge the area of the upper terrace underneath the STM tip increases and decreases periodically, which leads to a component proportional to $u_1 \sin \omega t$ in the tunneling current. By integration of the tunneling current over the entire surface one obtains for the signals at the mixing frequency $\Delta\omega$, at the step

$$I_{S,\Delta\omega} \propto \pi\kappa V_{\mathrm{mod}} e^{-2\kappa d}\Bigg\{ u_3(1+e^{-2\kappa h})\cos\Delta\omega - \Bigg[\frac{u_1}{\sqrt{\pi\kappa d}}\left(1-\frac{1}{4\kappa d}\right)+\frac{u_1}{\sqrt{\pi\kappa(d+h)}} \times\left(1-\frac{1}{4\kappa(d+h)}\right)e^{-2\kappa h}\Bigg]\sin\Delta\omega\Bigg\}, \tag{3}$$

and on the terrace

$$I_{T,\Delta\omega} \propto 2\pi\kappa V_{\mathrm{mod}} e^{-2\kappa d} u_3 \cos\Delta\omega, \tag{4}$$

with d being the tunneling distance and κ the reciprocal decay length of the electron wave function in the tunneling gap. The amplitude A of the mixing signal as well as its phase φ are given by

$$A \propto \pi\kappa V_{\mathrm{mod}} e^{-2\kappa d} u_3 \sqrt{P^2+Q^2}, \tag{5}$$

$$\varphi = \arctan\left(\frac{Q}{P}\right), \tag{6}$$

with

$$P = 1 + e^{-2\kappa h}, \tag{7}$$

$$Q = -\frac{1}{\sqrt{\pi\kappa d}}\Bigg[\left(1-\frac{1}{4\kappa d}\right) + \sqrt{\frac{d}{d+h}}e^{-2\kappa h}\left(1-\frac{1}{4\kappa(d+h)}\right)\Bigg]\frac{u_1}{u_3}. \tag{8}$$

Figure 5 shows plots of the relative amplitude A_S/A_T and the phase-shift $\Delta\varphi$ as a function of the step height h with the STM tip being 1 nm above the step edge. For the calculations we used a typical reciprocal decay length of $\kappa = 10\ \mathrm{nm}^{-1}$ and different eccentricity values β. We remark that the sign of the phase shift is positive (negative) when the SAW is approaching an ascending (descending) step. As expected, the contribution of the lateral step movement to the measured amplitude and phase is strongest for longitudinal SAWs, i.e., with β close to 90°. For $\beta = 88°$, $\Delta\varphi$ at a monostep of Au(111) with $h = 0.236$ nm is about 79° and A_S is increased by a factor of about 2.5 with respect to A_T. For smaller β the relative amplitude drops rapidly and assumes values below 1 for $\beta < 82°$. In the case of the Rayleigh wave ($\beta = 35.1°$) A_S is smaller than A_T by a factor of 0.8 and the corresponding phase shift is reduced to 6.8°. Both values are actually in reasonable agreement with the experimental values found at monostep S_1, namely, $A_S/A_T \sim 0.85$ and $\Delta\varphi \sim 9°$.

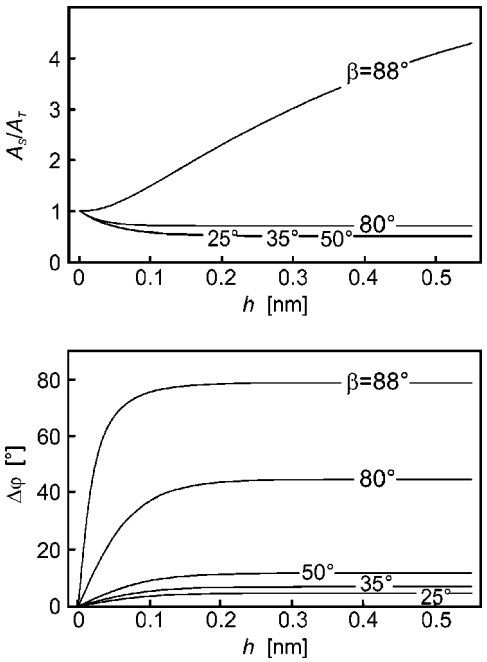

FIG. 5. Relative amplitude A_S/A_T and phase-shift $\Delta\varphi$ as a function of the step height h with the STM tip being 1-nm above the step edge and $\kappa = 10\ \mathrm{nm}^{-1}$; A_T and A_S are the amplitude of the mixing signal at the terrace and step, respectively.

C. Geometrical shape of the STM tip

Our analysis so far shows that the SAW-induced signals are not described properly by the two existing models, which actually represent the two limiting cases of small and large length scales. Obviously, for nanoscale objects of intermediate size (e.g., steps with heights of 1–2 nm) other effects, not included in the two models, play a role as well. A very important parameter in STM investigations is the shape of the STM tip, which is well known to decisively influence lateral resolution. In the following we discuss, in more detail, how the tip shape will affect the outcome of a SAW-STM experiment.

Figure 6(a) sketches a (perfectly sharp) STM tip which scans a horizontal terrace as well as the facet of a 1–2-nm high step. Away from the step, mainly the tip apex is involved in the tunneling process, which collects the tunneling current from a region indicated by the gray cone in Fig. 6(a), left. When both terrace and step are formed by (111) planes as, e.g., in Fig. 2, the inclination angle of about 70° becomes comparable with the slope of the STM tip. Therefore, when the tip is scanning the step, the tunneling cone is shifted from its apex to the side facing the step [Fig. 6(a), right]. However, although now a much larger number of tip atoms is involved in the tunneling process, the dc tunneling current remains unchanged, because it is kept constant in the con-

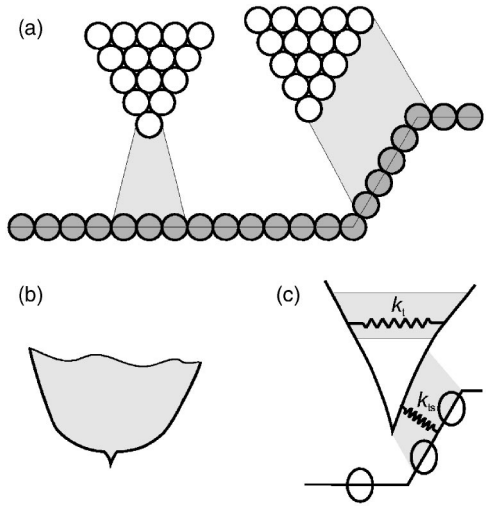

FIG. 6. (a) Schematic illustration of the influence of the STM tip shape on the SAW detection: on a horizontal terrace away from steps (left) and at a step, which is several atomic layers high and exhibiting a tilt angle comparable to that of the tip side (right); the tunneling regime, from which the main part of the tunneling current is collected, is shaded in gray in both cases. (b) Possible shape of a real STM tip. (c) Schematic illustration of a possible SAW- induced tip oscillation; the force constants k_t and k_{ts} account for the bending mode of the tip and for the tip-surface interaction, respectively.

stant current mode. The tip-sample distance is adjusted by the STM controller to guarantee that $n_{\mathrm{side}}(\kappa_S/d_{\mathrm{side}}) \times \exp(-2\kappa_S d_{\mathrm{side}}) \approx n_{\mathrm{apex}}(\kappa_T/d_{\mathrm{apex}})\exp(-2\kappa_T d_{\mathrm{apex}})$. d_{apex} and d_{side} are the tunneling distances when the tip scans mainly with its apex or side, respectively, n_{apex} and n_{side} give the number of tip atoms (mainly) involved. The change in the tunneling geometry affects also the measurement of the high-frequency signal. Depending on whether the tunneling current is collected mainly from the tip apex or its side one obtains for the amplitude of the mixing signal [e.g., by using Eq. (4)],

$$A_{\mathrm{side}} = \frac{d_{\mathrm{side}}}{d_{\mathrm{apex}}} A_{\mathrm{apex}}. \tag{9}$$

For the tip shape in Fig. 6(a) $n_{\mathrm{apex}}=1$ and $n_{\mathrm{side}}=15$. With $\kappa_S=\kappa_T=10\ \mathrm{nm}^{-1}$ and $d_{\mathrm{apex}}=1$ nm we obtain for $d_{\mathrm{side}}/d_{\mathrm{apex}}=1.13$, which corresponds to an increase of the amplitude of the mixing signal by 13% compared to the value calculated, e.g., by Eq. (1). The mixing signal at monosteps (Sec. IV B) is also affected by a change in the tunneling geometry, whereby in that case a decrease of the amplitude is more likely. It needs to be emphasized, however, that the tip shape of Fig. 6(a) is an ideal one, used to simplify the discussion. In reality, STM tips are more blunt with the mesoscopic shapes resembling rather the one sketched in Fig. 6(b), where the number of tunneling atoms might even be larger. A quantitative evaluation of the SAW-induced signal therefore requires not only a detailed knowledge of the structural features of the surface but also of the shape and electronic properties of the STM tip.

D. STM tip-surface interaction

In this section we want to discuss the influence of tip-surface interactions in SAW-STM experiments. It is well known that attractive and repulsive forces between the tip and surface play an important role in scanning probe techniques. They are utilized for the controlled manipulation of single atoms[12–14] and molecules[15] with the STM and can be measured by AFM (Refs. 16 and 17) via the bending of the tip carrying cantilever. Direct measurements of the forces involved in STM have been performed by Dürig and co-workers.[18–20] The results of these studies actually suggest that for the geometry sketched in Fig. 6(a), where many tip atoms come into close contact with the surface, the involved attractive forces may be strong enough to induce a small but significant deflection of the (thin) tip end. The magnitude of this effect can be estimated by a simple spring model, with k_{ts} and k_t being the force constants of the tip-surface interaction (F_{ts}) and of the restoring force of the tip (F_t), respectively [see Fig. 6(c)]. For small displacements the forces can be assumed to be linear in distance, i.e., $F_{ts}=F_0+k_{ts}(x_t-k_s)$ and $F_t=-k_t x_t$. x_t denotes the tip displacement upon bending, $x_s=A_{\mathrm{SAW}}\cos(\omega_{\mathrm{SAW}}t)$ describes the SAW-induced surface oscillation perpendicular to the surface, and F_0 is the attractive force experienced by the tip in the absence of a SAW. A simple calculation yields the resulting amplitude of the tip oscillation A_{tip}:

$$A_{\mathrm{tip}} = -\frac{\frac{k_{ts}}{m}}{\frac{k_t}{m}-\frac{k_{ts}}{m}+\omega_{\mathrm{SAW}}^2} A_{\mathrm{SAW}} \approx -\frac{k_{ts}}{k_t-k_{ts}} A_{\mathrm{SAW}}, \tag{10}$$

where $k_{ts}/m=\omega_B^2$ is the squared resonance frequency of the bending mode of the vibrating tip end. The magnitude of ω_B can be estimated from the resonance frequency of a nanoscale cantilever beam[21] $2\pi\nu_{\mathrm{CB}} \approx (w/l^2)\sqrt{Y/\rho}$ with Y, ρ, w, and l being its Young's modulus, density, width, and length, respectively. Inserting, for instance, $Y=77$ GPa and $\rho=19.300\ \mathrm{kg/m^3}$ of Au, which is the very likely material at the apex of a STM tip scanning on a thin Au film, and taking reasonable dimensions of $w=1$ nm and $l=2$ nm we obtain for $\omega_{\mathrm{CB}} \sim 500$ GHz. The bending frequency of a molecule adsorbed at the tip apex and involved in tunneling (e.g., CO) is even higher (10^{12}–10^{13} Hz). Since in our experiment ω_B is more than two orders of magnitude larger than the frequency of the Rayleigh wave ($\omega_{\mathrm{SAW}}=2\pi\cdot 246$ MHz), ω_{SAW} can be neglected in the denominator of Eq. (10). The calculation shows that the amplitude of the tip oscillation is determined by the relative magnitude of the two involved interactions described by the force constants k_{ts} and k_t and becomes relevant, when k_{ts} is of the same order of magnitude as k_t.

In order to get an estimate of the magnitude of k_{ts} we refer to a sophisticated STM study by Cross *et al.*, who combined the movable STM tip with a bendable sample and characterized the tip geometry on the atomic level by field ion microscopy.[20] For a tungsten tip with a trimer on its apex, which is tunneling on a 200-nm-thick Au film, the (reversible) force-distance curves reveal linearly increasing attractive forces at distances smaller than ~2 nm until the forces

become repulsive at distances below ~0.3 nm. The slope in the attractive region is ~3 N/*m*. We remark that force gradients in force-distance curves measured by AFM usually are higher. For example, for an oxygen-free Si tip scanning graphite a force gradient of 15 N/m was obtained at tip/sample distances of about 1 nm.[17] However, the depth of the measured potential indicated that more than one tip atom was interacting with the sample surface in that experiment. Taking $\omega_{CB}=\sqrt{k/m}$ with $m=\rho l w^2$ to estimate the force constant for the bending mode of the tip we obtain $k_t \sim 10$ N/m.

Obviously k_{ts} and k_t indeed may be of the same order of magnitude, leading to comparable amplitudes of the SAW-induced tip and surface movement. According to Eq. (10) there is a phase shift of 180°, which means that the amplitude of the tunneling gap oscillation is increased by the tip movement. We remark that due to the exponential characteristics of the current-distance dependence, A_{tip} being ~3.5% of A_{SAW} is already sufficient to account for a doubling of the mixing signal.

E. Local work function

Finally, we want to address the role of the work function in more detail, which is already included implicitly in the mechanisms discussed above. It is well known that the work function not only influences the magnitude of the tunneling current[22–24] but also affects the amplitude in the geometric model (Sec. IV A), as well as the amplitude and phase signals obtained in Sec. IV B, and Eqs. (3) and (4). For a given material the work function depends on the detailed crystallographic structure of the surface[25,26] and is modified by adsorbates.[27] Furthermore, electron smoothing due to the Smoluchowski effect[28] can reduce the work function locally at the step edges. The overall difference in the work function reported in the literature is about 25–30%, which leads to changes in the reciprocal decay length $\kappa \propto \sqrt{\phi}$ about 5%. This leads to a change of the amplitude at extended terraces by about 2% when inserted, e. g., into Eqs. (3) and (4).

V. SUMMARIZING DISCUSSION

Our SAW-STM investigation of SAWs at steps with heights of several atomic layers revealed that the detected amplitude and phase signals at the steps can no longer be described by the geometrical model of Chilla *et al.* (Sec. IV A). This model was proposed originally for highly corrugated surfaces exhibiting extended facets with small tilt angles, where it quantitatively reproduces the experimental amplitude and phase contrast. However, particularly the strong enhancement of the amplitude signal at steps that are only several atomic layers high is contradictory to the effect of a plain geometrical projection. Our analysis shows that several other possible mechanisms proposed and discussed in Sec. IV—nanoscale feature size, geometrical tip shape, and local changes in work function—certainly influence the magnitude and phase of the SAW-induced signal, but their contribution is too small for a satisfying explanation. Our results provide strong evidence that the SAW drives an oscillatory movement of the end of the STM tip, when it scans at a step with comparable inclination angle and a height similar to the tunneling distance (1–2 nm). At this conditions the attractive surface forces experienced by the tip can compete with the elastic forces involved in tip bending. The resulting tip movement increases the tunneling gap oscillation and is responsible for the enhanced amplitude of the SAW-induced mixing signal at steep steps. This explanation is corroborated by Fig. 7 which shows SAW-STM results of a surface area exhibiting two steps with different inclination angles. Whereas the amplitude signal [Fig. 7(b)] is strongly enhanced in scans of the steep step in the lower part of Fig. 7(a) (see also linescan A), it is similar to that of the terraces at the less inclined step in the upper part of Fig. 7(a) (see linescan B). Note that in this experiment the two steps were imaged at identical tunneling parameters, thus excluding the effects of the tunneling voltage and current, tip shape, excitation voltage of the SAW, etc. The tip itself was quite sharp as close-packed atomic rows are resolved in Fig. 7. However, the amplitude signal is enhanced only at the steep step, thus indicating that the tunneling cone indeed moves from the tip apex to its side, where a larger number of atoms can attract the tip. From our experiments we conclude that the STM tip follows the surface oscillation only at the steep step, but not at the flat one or on the terraces. We want to remark that increased signals at steps are commonly observed in AFM images, when the scanning speed is too high for the electronics to keep the preset tunneling distance constant. This is definitely not the case in the SAW-STM experiments of the present study, where the scanning time is about 40 times larger than that of typical STM images. Note also that the amplitude of a SAW is the result of the concerted oscillation of all the atoms in a surface slab approximately as thick as one SAW wavelength ($A_{SAW} \sim 15$ μm). Therefore, the amplitude of individual surface atoms is very small, about $10^{-4} A_{SAW}$, whereas A_{tip} is of the same order as A_{SAW}.

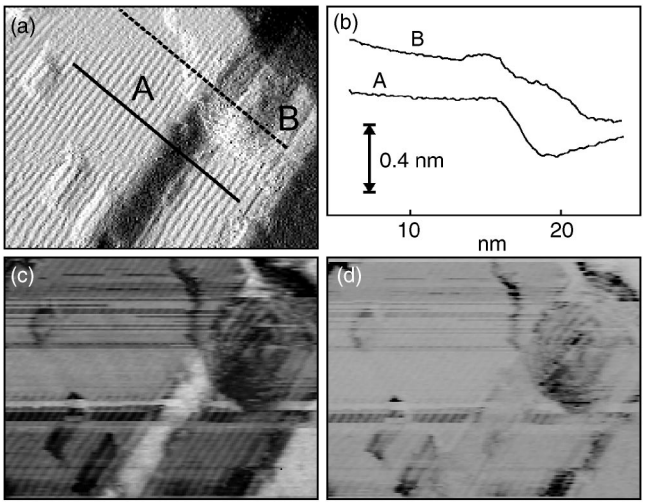

FIG. 7. (a) 34×25 nm^2 differentiated STM image (left) of a 100-m-thick Au film on *Y*-cut $LiNbO_3$ as well as of two linescans of steps (right) marked by A and B in the topview. b) Corresponding amplitude and (c) phase image of a Rayleigh wave, both recorded simultaneously with topography. Note the strong enhancement of the amplitude contrast at the steep step (linescan A).

In conclusion, STM has proven in the past to be a powerful technique to probe and image the high-frequency wave

fields of SAWs on a length scale well below the SAW wavelength. Whereas on mesoscopically corrugated surfaces the SAW- induced signal can be reproduced reliably by using the structural information of the STM topography, our study reveals that a variety of additional mechanisms have to considered as well, when the feature size on the surface approaches the dimensions of a few nanometers. In fact, the quantitative evaluation of the SAW-induced signal then requires not only a detailed knowledge of the surface structure but also of the shape and electronic properties of the STM tip. Our analysis of the SAW-STM data of nanoscale surface structures is not only important for future investigations of nanoelasticity but also for other high frequency applications of the STM, e.g., time-resolved investigations of the magnetization reversal where due to magnetostriction the surface will oscillate as well.

ACKNOWLEDGMENTS

We wish to thank D. M. Schaadt and Th. Hesjedal for helpful discussions. The work was supported by the EFRE and the NEDO International Joint Research Program "Nanoelasticity."

[1]D. Royer and E. Diulesaint, *Elastic Waves in Solids I* (Springer, Berlin, 2000).
[2]J. P. Monchalin, IEEE Trans. Ultrason. Ferroelectr. Freq. Control **33**, 485 (1986).
[3]E. Chilla, W. Rohrbeck, H.-J. Fröhlich, R. Koch, and K. H. Rieder, Appl. Phys. Lett. **61**, 3107 (1992).
[4]T. Hesjedal, E. Chilla, and H.-J. Fröhlich, Appl. Phys. Lett. **69**, 354 (1996).
[5]P. U. Voigt and R. Koch, J. Appl. Phys. **92**, 7160 (2002).
[6]J. Yang, P. U. Voigt, and R. Koch, Appl. Phys. Lett. **82**, 1866 (2003).
[7]O. Kolosov and K. Yamanaka, Jpn. J. Appl. Phys., Part 2 **32**, L1095 (1993).
[8]K. Yamanaka, H. Ogiso, and O. Kolosov, Appl. Phys. Lett. **64**, 178 (1994).
[9]T. Hesjedal, E. Chilla, and H.-J. Fröhlich, Appl. Phys. Lett. **70**, 1372 (1997).
[10]E. Chilla, W. Rohrbeck, H.-J. Fröhlich, R. Koch, and K. H. Rieder, Ann. Phys. **3**, 21 (1994).
[11]P. U. Voigt, S. Krauß, E. Chilla, and R. Koch, J. Vac. Sci. Technol. A **19**, 1817 (2001).
[12]D. M. Eigler and E. K. Schweizer, Nature (London) **344**, 524 (1990).
[13]L. Bartels, G. Meyer, and K.-H. Rieder, Phys. Rev. Lett. **79**, 697 (1997).
[14]S.-W. Hla, K.-F. Braun, and K.-H. Rieder, Phys. Rev. B **67**, 201402(R) (2003).
[15]F. Moresco, G. Meyer, K.-H. Rieder, H. Tang, A. Gourdon, and C. Joachim, Phys. Rev. Lett. **86**, 672 (2001).
[16]S. P. Jarvis, H. Yamada, S.-I. Yamamoto, H. Tokumoto, and J. B. Pethica, Nature (London) **384**, 247 (1996).
[17]H. Hölscher, W. Allers, U. D. Schwarz, A. Schwarz, and R. Wiesendanger, Phys. Rev. Lett. **83**, 4780 (1999).
[18]U. Dürig, J. K. Gimzewski, and D. W. Pohl, Phys. Rev. Lett. **57**, 2403 (1986).
[19]U. Dürig, O. Züger, and D. W. Pohl, Phys. Rev. Lett. **65**, 349 (1990).
[20]G. Cross, A. Schirmeisen, A. Stadler, P. Grütter, M. Tschudy, and U. Dürig, Phys. Rev. Lett. **80**, 4685 (1998).
[21]W. F. Stokey, *Shock and Vibration Handbook* (McGraw-Hill, New York, 1989), pp. 7.1–7.44.
[22]G. Binnig and H. Rohrer, Surf. Sci. **126**, 236 (1983).
[23]N. D. Lang, Phys. Rev. B **37**, 10395 (1988).
[24]L. Olesen, M. Brandbyge, M. R. Sørensen, K. W. Jacobsen, E. Lægsgaard, I. Stensgaard, and F. Besenbacher, Phys. Rev. Lett. **76**, 1485 (1996).
[25]J. F. Jia, K. Inoue, Y. Hasegawa, W. S. Yang, and T. Sakurai, Phys. Rev. B **58**, 1193 (1998).
[26]C. J. Fall, N. Binggeli, and A. Baldereschi, Phys. Rev. Lett. **88**, 156802 (2002).
[27]G. Dujardin, F. Rose, and A. J. Mayne, Phys. Rev. B **63**, 235414 (2001).
[28]R. Smoluchowski, Phys. Rev. **60**, 661 (1941).